Fabrication of Nanoporous Structures in Block Copolymer Using Selective Solvent Assisted with Compressed Carbon Dioxide

Rui Zhang[†] and Hideaki Yokoyama*

Department of Advanced Materials Science, Graduate School of Frontier Sciences, The University of Tokyo, 603 Transdisciplinary Sciences Building, 5-1-5 Kashiwa-no-ha, Kashiwa, Chiba 277-8561, Japan

Received January 19, 2009; Revised Manuscript Received March 31, 2009

ABSTRACT: The fabrication of nanostructured thin films is important in a variety of applications. This article presents a fabrication method for introducing nanoscopic pores into polymeric thin films of block copolymers. As a model of this method, poly(styrene-*b*-2-vinylpyridine) (PS-PVP) thin film of which the original thickness is about 150 nm was employed with mixtures of methanol and CO_2. Neither methanol nor CO_2 alone can introduce nanopores into the PS-PVP thin films; however, the mixtures of methanol and CO_2 can effectively localize methanol into PVP domains and leave nanopores after being removed. Methanol alone has a strong affinity for PVP blocks and potentially swells the PVP domains, but the glassy PS matrix prevents them from swelling. Therefore, it is essential for the successful introduction of nanopores to reduce the glass-transition temperature (T_g) of PS by plasticizing with CO_2. Compressed CO_2, which reduces the T_g of PS, can quickly be removed from the mixture upon depressurization and increases the T_g of PS to prevent nanopores from collapsing. The size of the nanopores can be successfully adjusted by changing the pressure of CO_2. On our experimental time scale, the morphologies were not equilibrium, and the resultant nanoporous structures depend on the initial morphologies before the process.

Introduction

Nanostructure has received increased attention in both academic and industrial fields.[1] However, the production of large-area structured surfaces with features on the nanometer scale still remains a challenge for conventional photolithography.[2] Nanometer scale patterns based on self-assembly have been considered as alternatives for replacing high-resolution lithographic technologies. Block copolymers as templates have been seriously considered for nanotechnological applications because of not only the scale of the nanodomains but also the convenient tunability of size, shape, and periodicity by changing their molecular parameters.[3−8] The drawback of the block copolymer templating is that available size, shape, and symmetry are restricted by the molecular architecture of block copolymers so that fine-tuning requires precisely controlled polymerization.

Liquid and supercritical CO_2 are inexpensive, nontoxic, and nonflammable fluids for materials synthesis and processing.[9] The particularly attractive properties of supercritical CO_2 are gaslike diffusivities, the continuously tunable solvent power and selectivity, and the complete elimination at the end of the process.[10] In the past years, CO_2 has been utilized as a particularly versatile medium for the preparation of porous materials because of its high diffusivity, low interfacial tension, and excellent wettability of surfaces.[11−13] In particular, microcells, cells with a diameter on the order of micrometer, attracted great interest. However, the accessible minimum size of the features in the conventional CO_2 process, in which CO_2 is introduced into polymeric monoliths and quickly depressurized to introduce foams, is limited to approximately 1 μm. Our group has demonstrated a method with CO_2 to fabricate optically transparent nanocellular polymeric materials using fluorinated block copolymers as templates for CO_2 foams. CO_2 was used as a porogen to introduce nanometer cells and pores in the nanodomains of bulk and thin film of block copolymers having fluorinated blocks.[14−17] The key to the successful introduction of nanometer cells and pores is selective swelling of the CO_2-philic fluorinated block domains with CO_2. After complete removal of CO_2, the volume occupied by CO_2 turns into empty voids.

Fluorinated block copolymers are very effective in localizing CO_2 in their fluorinated nanodomains. However, the synthesis and the number of available fluoromonomers are very limited. An alternative approach using nonfluorinated block copolymers as templates to obtain similar nanostructures is desired. However, because of the low dielectric constant of CO_2, most of ordinary polymers are immiscible with CO_2.

However, a variety of ordinary solvents are available to swell particular domains of block copolymers. Perpendicularly oriented cylindrical morphologies have been converted to porous structures by exposing selective solvents to the vertically aligned cylindrical domains.[18−21] Such surface reconstruction methods are limited not only to the minority domains directly exposed to the surface but also to the domains near the surface that can redistribute minority blocks to the surface. To introduce open nanoporous structure into relatively thick films or monolithic materials with embedded morphologies by this selective swelling method, the matrix domains must be rubbery to allow the dispersed domains to swell. However, when the solvent is removed, the matrix domains must be glassy to retain the swollen minority domains and to prevent collapsing. In our previous studies of poly(styrene-*b*-perfluorooctylethyl methacrylate) with pure CO_2, reducing temperature before depressurization was the key to the successful fabrication of nanocellular structure[14] utilizing the characteristics that PS is rubbery at 60 °C but glassy at 0 °C in pure CO_2.

In this work, we report an efficient approach to introduce nanopores into polymeric films of poly(styrene-*b*-2-vinylpyridine) (PS-PVP) with mixtures of methanol and CO_2. Methanol is a good solvent for hydrophilic polymers such as PVP and a nonsolvent for PS, whereas CO_2 does not dissolve but plasticizes both PVP and PS with weak selectivity toward PVP.[22] PVP block domains are expected to swell in methanol, similar to fluorinated block domains in CO_2. However, because PS is

* To whom correspondence should be addressed. E-mail: yokoyama@molle.k.u-tokyo.ac.jp. Tel/Fax: +81-4-7136-3766.

[†] Current address: Functional Thin Films group, Organic Nanomaterials Center, National Institute for Materials Science (NIMS), Tsukuba, Ibaraki, Japan.

10.1021/ma900123e CCC: $40.75
Published on Web 04/16/2009

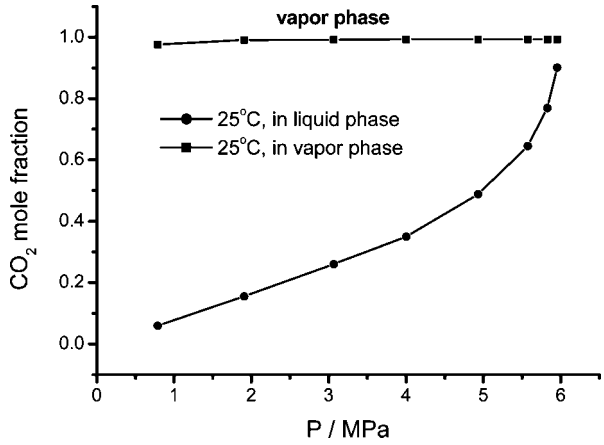

Figure 1. Dependence of CO_2 mole fraction in methanol on the CO_2 pressure at 25 °C. (The data are taken from ref 24).

glassy in methanol, swelling of PVP surrounded by PS is hindered. Compressed CO_2 added to methanol drives PS to a rubbery state by plasticizing and allows PVP domains to swell. CO_2 can easily be removed from the mixtures simply by reducing pressure so that PS becomes glassy to retain the nanoporous structures. By utilizing methanol assisted by compressed CO_2 as a tunable solvent, nanopores are successfully introduced, even in embedded domains inside the films.

Experimental Section

Poly(styrene-*b*-2-vinyl pyridine) (PS-PVP) was synthesized by sequential anionic polymerization. The details of the polymerization have been described elsewhere.[23] The molecular weights of PS and PVP blocks are 44 300 and 18 400 g mol^{-1}, respectively. The PS-PVP copolymer was dissolved in toluene (Wako), and thin films were prepared by spin-casting the solution onto the Si substrates (Shinetsu). The 6-inch silicon wafers were used as received and were cut into 10-mm-square pieces. Film thickness was controlled by concentration of the solutions and rotating speed. The thicknesses of the samples were about 150 nm. Some PS-PVP thin films were heated to 180 °C under high vacuum (10^{-5} Pa) for 24 h before the process to introduce nanopores.

A stainless steel high-pressure vessel for CO_2 processes was connected to a high-pressure liquid chromatography pump (JASCO PU-2086 plus) with a cooling head and to a back-pressure regulator (JASCO SCF-Bpg). Wafers coated with PS-PVP were loaded into the high-pressure vessel. Methanol was added to the vessel so that the specimens would be completely submerged. The vessel was placed in a temperature-controlled water bath. After the temperature reached 25 °C, CO_2 was pumped into the vessel, and the pressure was maintained with the back-pressure controller. The maximum pressure used was 6 MPa. At the end of the process, pressure was released at a rate of 0.5 MPa/min. After complete removal of CO_2, the specimens were still immersed in methanol. Subsequently, methanol was completely removed from the specimens in a vacuum for 1 h.

At relatively low pressure, CO_2 and methanol show two-phase coexistence. The mole fractions of CO_2 in gas and liquid phases are plotted as a function of CO_2 pressure for the CO_2/methanol binary system in Figure 1.[24]

Film thickness and refractive index were measured with a JASCO M-220 ellipsometer with incident light in a wavelength range of 400−800 nm at an incident angle of 60° with respect to the surface normal. Because the size of nanostructures templated by the nanodomains of PS-PVP is much smaller than the wavelength of light, we assume that effective medium approximation is valid. The changes in both thickness and refractive index were observed and were used to compute the porosities with two different definitions: A porosity, V_t, can be defined by the increment of thicknesses before (t) and after the process ($t + \Delta t$)

$$V_t = \Delta t/(t + \Delta t) \tag{1}$$

and V_n can be defined by refractive index according to the Lorentz−Lorenz equation

$$\frac{n_f^2 - 1}{n_f^2 + 2} = (1 - V_n)\frac{n_s^2 - 1}{n_s^2 + 2} \tag{2}$$

where n_f and n_s are the refractive indices of a nanoporous film and solid block copolymer film, respectively.

Etching to expose embedded nanostructures inside of the films to the surface for subsequent scanning electron microscopy (SEM) and atomic force microscopy (AFM) was carried out with a reactive ion etcher (SAMCO compact etcher FA-1) with a CF_4 flow rate of 2 mL/min, a pressure of 10 Pa, and a power density of 10 W/cm^2. Under this condition, the etching rate for PS-PVP copolymer thin films was about 0.8 nm/s. AFM measurements were performed in the tapping mode with a Seiko Instrument SPA 300HV. We used silicon tips (spring constant of 22 N/m) to image the topography of the surface. SEM images were obtained using an environmental scanning electron microscope (ESEM) (Philips XL20 ESEM-FEG) equipped with a field-emission gun under high-vacuum conditions. A 10 keV electron beam was used for the observations. No conductive coatings were applied to the specimen surfaces to avoid possible artifacts.

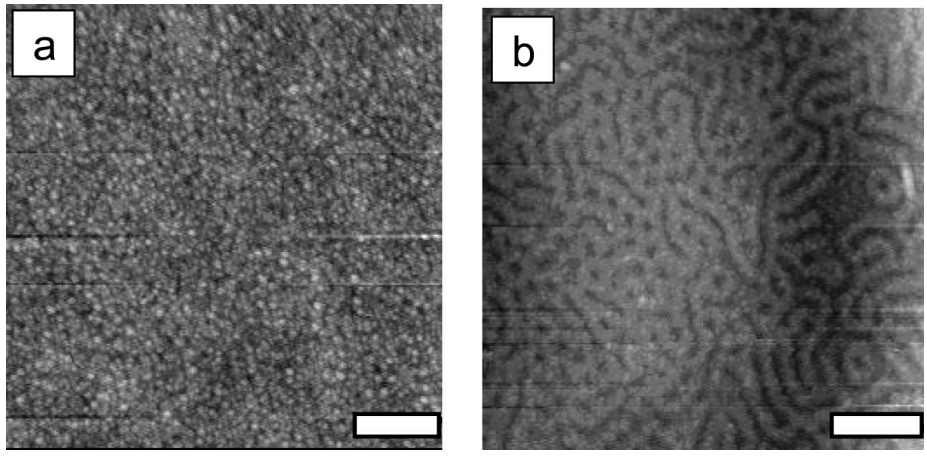

Figure 2. AFM topographic images of PS-PVP thin films. The scale bars indicate 200 nm. (a) Topographic image with a full-scale height of 12 nm of an as-cast PS-PVP film after etching 40 nm by RIE. (b) Topographic image with a full-scale height of 22 nm of the PS-PVP film after thermal annealing at 180 °C for 24 h and subsequent 40 nm etching. The height was scaled from black (low) to white (high) with the given full scales.

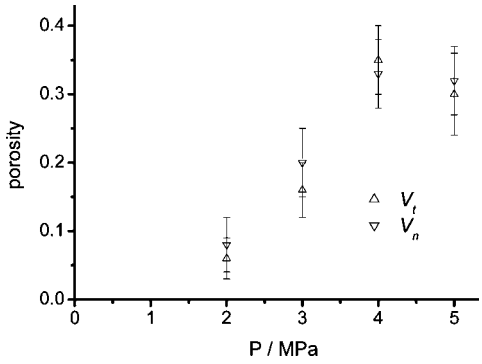

Figure 3. Dependence of the porosity on the CO_2 pressure for the PS-PVP thin films after exposure to mixtures of methanol and CO_2. The porosities V_t and V_n were estimated from the changes in film thickness and refractive index, respectively.

Results and Discussion

Domain Structures in As-Cast and Annealed Films. PS-PVP thin films were spun-cast from toluene solutions. We first checked the morphology of the PS-PVP films before the nanoporous process. As shown in the AFM topographical image in Figure 2a, no well-defined nanodomains were found after the reactive ion etching (RIE) with CF_4 gas under the conditions described in the Experimental Section. RIE has been proven to etch away PS-PVP films with a controlled rate and enhance the contrast due to the slightly different etching rate of PS and PVP.[25] Under several different etching conditions and therefore at different depths, no well-defined domain structures were found in the as-cast films. Because of the rapid evaporation of toluene during the spin-casting process, we found only sporadic dark circles of PVP domains, which are not layered parallel to the surface. However, the film thermoannealed at 180 °C for 24 h shows cylindrical domains of PVP, which are the expected morphology on the basis of the volume fraction of PVP, which appears dark in Figure 2b. In the as-cast film, PVP domains are not clearly formed due to rapid evaporation of the solvent. However, after thermal annealing, PVP domains formed cylindrical domains. Because of the strong repulsive interaction between PS and PVP and relatively high molecular weight, no long-range order is achieved even after thermal annealing. It should be noted that SEM did not observe such topographic pattern of the films made by reactive etching because the topographical contrast is too small.

Effect of Pure Methanol and CO_2. We used the aforementioned thin films with and without thermal annealing as templates for nanoporous structures using selective swelling with a mixture of methanol and CO_2. As a reference, a PS-PVP film was immersed in pure methanol at 25 °C for 5 h. Both the thickness and refractive index were measured before and after the process. The thicknesses of the films before and after immersing in methanol were 148.1 ± 2.7 and 149.7 ± 1.9 nm, and the refractive indices of those were 1.53 and 1.53, respectively. The estimated porosities, V_t and V_n, which were defined in eqs 1 and 2 are zero. This reference experiment indicates that pure methanol cannot swell PVP domains surrounded by glassy PS domains, although methanol is a good solvent for PVP. Because toluene, which was used for spin-casting, is a good solvent for PS but a poor solvent for PVP, the surface of the films are fully covered by PS. In addition, thermal annealing drives PS to the surface to reduce the surface energy. Also, PS is a major component in the PS-PVP copolymer and forms solid skeleton (matrix) domains surrounding the PVP domains. Such PS surface layer as well as continuous PS domains in the films prevent PVP domains from swelling.

To evaluate the effect of pure CO_2 on the capability of introducing nanoporous structures, we processed the PS-PVP films in pure CO_2 at 4 and 6 MPa for 1 h at 25 °C. The values of porosities V_t and V_n after the process were at most 0.04 at 4 MPa and 0.03 at 6 MPa, which are negligibly small relative to the experimental precision. Because it is known that PS as well as PVP can be swollen by CO_2, the film shrinks back during removal of CO_2. In conclusion, neither pure methanol nor pure compressed CO_2 can introduce nanopores to the embedded domains of PVP in the PS-PVP thin films. In our previous report of successful introduction of nanocellular and nanoporous structures using fluorinated block copolymers and CO_2,[14−17] not only the affinity of CO_2 to the minority block domains but also the effective plasticization with CO_2 of the matrix domains of majority block, that is, PS, were found to be essential. In the case of PS-PVP, methanol is a good solvent for the minority PVP block, but it does not effectively plasticize the major PS block. Therefore, the glassy PS matrix domains prevent the PVP domains from swelling with methanol. This result with methanol is quite different from the previous report from Guarini and Xu, in which perpendicularly oriented cylindrical domains in poly(styrene-*b*-methyl methacrylate) (PS-PMMA) were successfully swollen by the selective solvent and the nanoporous surface was successfully fabricated.[18−20] However, such phenomena are based on the surface reconstruction mechanism in which solvent-philic block chains are redistributed to the surface as a surface covering layer without deformation of non-solvent-philic domains. Therefore, such a method is limited to the case in which solvent-philic and non-solvent-philic domains are simultaneously exposed to the surface, and also, the film thickness is very thin. In our case, the surface of the PS-PVP is covered by PS domains to reduce the surface energy.[25] Therefore, it is not possible, at least on our experimental time scale, for methanol to penetrate the PS-PVP thin films and to swell the embedded PVP domains. However, CO_2 plasticizes the PS domains effectively and reduces the glass-transition temperature, T_g, to about 30 °C,[26] but the selectivity of CO_2 toward PVP is not strong enough to swell PVP significantly.[22,27] At 35 °C and in the pressure range of $P = 1.38$ to 10.34 MPa, 100 g of PS with $M_w = 71\,000$ absorbs 1.84 to 5.56 g of CO_2, whereas 100 g of PVP with $M_w = 65\,000$ absorbs 2.58 to 17.0 g of CO_2. Although PS-PVP films were swollen in CO_2 slightly more than PVP domains, the films appear to shrink back to the original thickness upon depressurization because of the lack of selectivity of CO_2, resulting in no porosity in the films.

Nanopores Fabricated by a Mixture of Methanol and Compressed CO_2. Methanol should swell PVP domains selectively if the solid PS matrix domains are effectively plasticized and become rubbery. To prove such a hypothesis, PS-PVP thin films were immersed in methanol and subsequently pressurized with CO_2. Under our experimental condition, two phases always coexist in the cell, and the sample always stays in the liquid phase. At 25 °C, the CO_2 mole fractions in the liquid phase increase with increasing pressure. After complete removal of CO_2, the specimens stayed in methanol, and then, methanol was completely removed in a vacuum.

Despite the negligible effect of either pure methanol or CO_2 on the formation of nanopores, we observed significantly increasing thickness and decreasing refractive index in PS-PVP thin films after the process with mixtures of methanol and CO_2. The porosities V_t and V_n estimated by eqs 1 and 2, respectively, are plotted in Figure 3 after exposure to the mixtures of methanol and CO_2 at 2, 3, 4, and 5 MPa. Apparent diameters of nanopores, which were estimated by taking the average of apparent opening of pores in the images as a function of pressure are plotted in Figure 4. Examples of the SEM images of PS-PVP thin films are shown in Figures 5. Note that the SEM images are the 2D

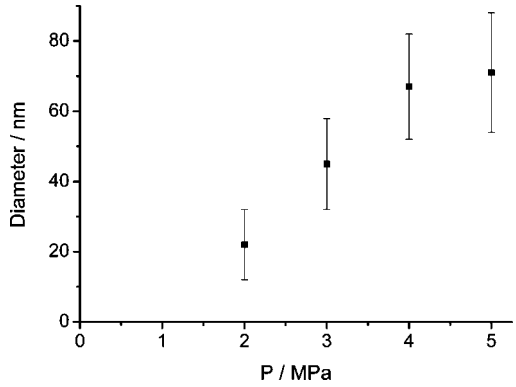

Figure 4. Dependence of apparent diameters of nanopores on CO_2 pressure in PS-PVP thin films determined by SEM.

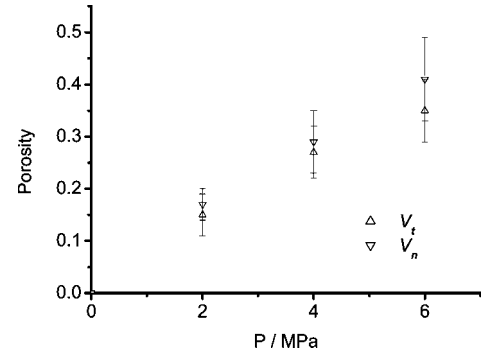

Figure 6. Dependence of the porosity after the CO_2 process on the CO_2 pressure for thermally preannealed PS-PVP thin films.

surface of a cut of 3D porous structures. Because of a lack of long-range order, we were not be able to reveal complete 3D porous structures, and we limit our discussion to the apparent shape and size of pores.

When CO_2 pressure was 2 MPa, sporadic nanopores appeared after depressurization and subsequent etching with RIE, as shown in Figure 5a, which is consistent with the low porosity, V_t, of 0.06. Note that the electron density contrast between PS and PVP is not strong enough to be visible in the SEM images in Figure 5a−d.[28] As pressure of CO_2 increased to 3 MPa, nanopores clearly appeared with an apparent diameter about 50 nm, as in Figure 5b, and porosity, V_t, increased to 0.16. As pressure further increases, connected tortuous pores become more evident. Pore size also increases with increasing pressure. The apparent diameter and porosity plateau at 5 MPa CO_2. From Figure 2, the mole fractions of CO_2 in the liquid phase are 16, 26, 35, and 49% at CO_2 pressures of 2, 3, 4, and 5 MPa, respectively. It is indicated that 35% of CO_2 is enough to soften PS domains to allow swelling of the dispersed PVP domains. Further increasing CO_2 pressure may not be advantageous for introducing nanopores because CO_2 is not as selective as methanol for PS and PVP,[22,27] as this experiment indicates. We speculate that the nanoporous processes at lower pressures are kinetically limited because of insufficient plasticization of the PS skeleton domains.

Effect of Initial Morphology on Nanoporous Structures. We have shown that as-cast films with poorly ordered morphology show tortuous nanopores, as in Figure 5, although the PS-PVP block copolymer presents cylindrical morphology in equilibrium. After thermal annealing at 180 °C for 24 h, the PS-PVP thin films show dark cylindrical domains of PVP with no long-range order, as in Figure 2b. We conducted the same series of experiments using the PS-PVP thin films that had been thermally preannealed before the process with CO_2. The porosities of PS-PVP films thermally preannealed and then processed with CO_2 at various pressures are plotted as a function of processing pressure in Figure 6. Porosity increases with

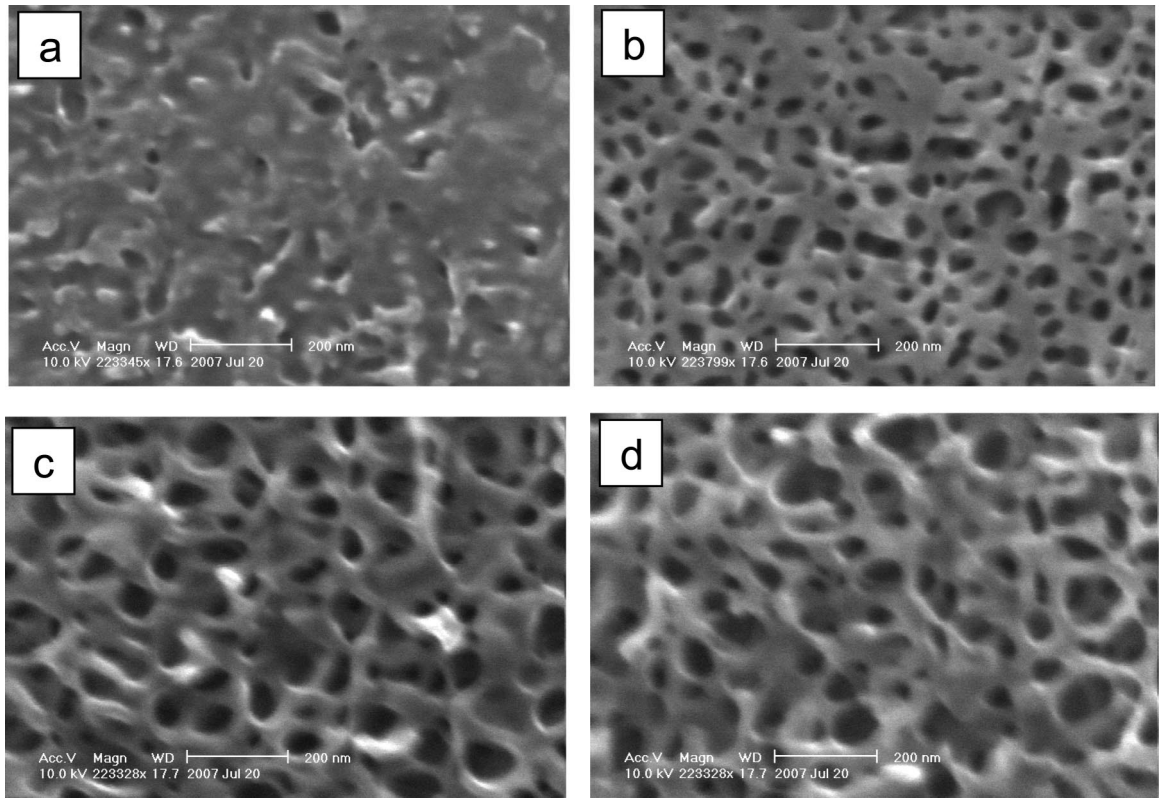

Figure 5. SEM images of PS-PVP processed in mixtures of methanol and compressed CO_2 with pressures of (a) 2, (b) 3, (c) 4, and (d) 5 MPa at 25 °C for 0.5 h and subsequent 48 nm etching by RIE.

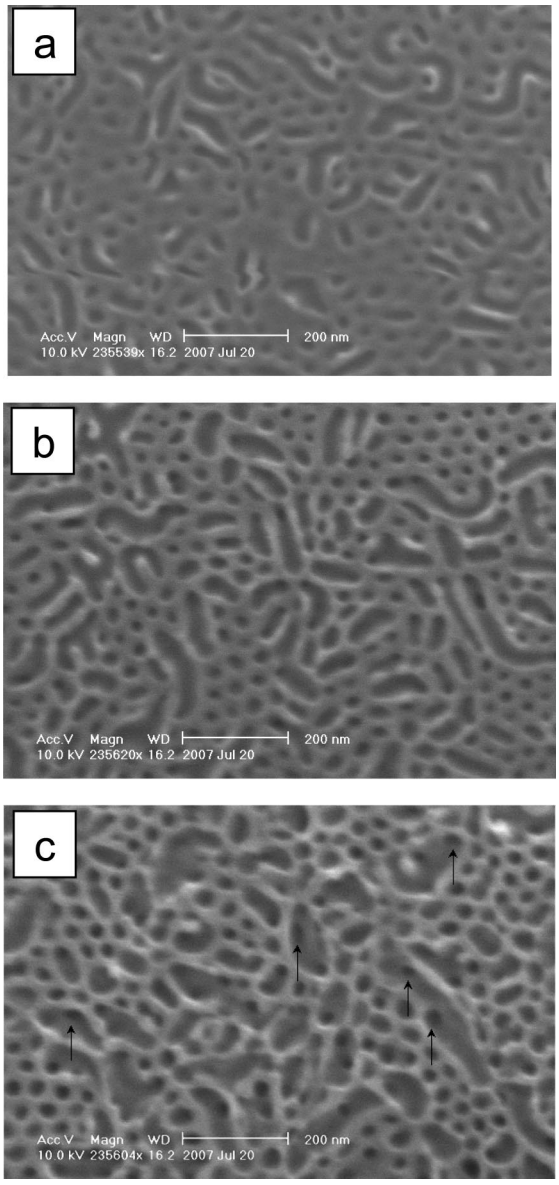

Figure 7. SEM images of PS-PVP films thermally annealed and processed in a mixture of methanol and CO_2 at various pressures ((a) 2, (b) 4, and (c) 6 MPa) at 25 °C for 0.5 h. The surfaces of specimens were etched 48 nm by RIE.

pressure qualitatively, similar to the case of as-cast films. The PS-PVP films with thermal annealing have a surface PS layer, which prevents methanol from being absorbed into PVP domains. Nevertheless, the added CO_2 to methanol effectively reduces the T_g of PS and selectively swells the PVP domains and introduces nanopores after CO_2 and then methanol are removed.

The original surfaces showed only sporadic pores; however, nanopores formed in the inner part of the films, as probed by SEM after RIE in Figure 7. The absence of nanopores at the original surfaces is the result of the surface-covering PS layer, which excludes PVP from the surface. The average apparent lengths of nanopores estimated from the SEM image are 149, 205, and 227 nm with CO_2 pressure at 2, 4, and 6 MPa, respectively. The average apparent diameters of nanopores are 41, 48, and 81 nm with CO_2 pressure at 2, 4, and 6 MPa, respectively. The lengths and diameters of nanopores are plotted as a function of CO_2 pressure in Figure 8. The diameters of the nanopores that appeared in the thermally annealed films are close to those in the as-cast films. The nanopores are templated from

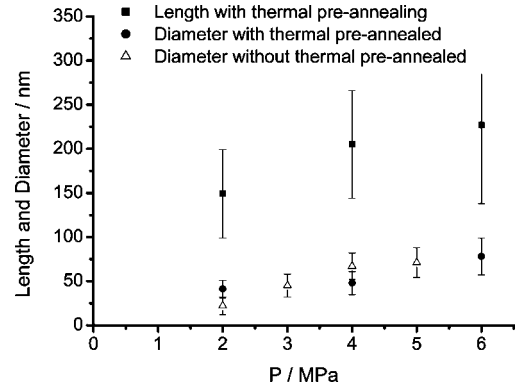

Figure 8. Apparent length and diameter of nanopores estimated from the SEM images as a function of CO_2 processing pressure. The error bars indicate standard deviations.

PVP domains, and hence the diameter of the nanopores has a strong correlation with the diameter of the cylindrical domains of PVP, whereas the size of the pores does not exactly match the diameter of the PVP domains because of selective swelling of PVP domains. However, the lengths of nanopores strongly depend on the degree of microphase segregation before selective swelling because such a long axis of pores was not clearly visible in the nanopores fabricated in as-cast films. Although the selective swelling in mixtures of methanol and CO_2 enhances the mobility of the PS-PVP copolymer by plasticizing PS and PVP domains and potentially induces longer-range order, the morphologies after the process are still kinetically restricted. The diameters of nanopores that are available under our experimental condition are close to those in equilibrium, but the lengths (connectivity) and packing symmetry of nanopores depend on the initial morphologies and hence are still kinetically restricted. The diameter of cylindrical domains instantly increases by swelling with methanol; however, growth of the lengths of nanopores requires the reorganization of PS-PVP chains, which are restricted by slow diffusion of PS-PVP molecules. As porosity increases, the nanopores begin to connect one another, as indicated by the arrows in Figure 7c. With the PS-PVP copolymer used in this study, the morphology did not change by swelling; however, morphological transition may potentially be induced by swelling, and nanoporous structures that are not simply templated from block copolymer morphology may be accessible using the same methodology. It should also be noted that this methodology is not limited to thin films but is potentially applicable to monolithic specimens. We are currently extending this methodology for monolithic specimens.

Conclusions

A facile, reproducible method of introducing nanopores into thin films of which the original thickness is about 150 nm has been developed using PS-PVP templates and mixtures of methanol and CO_2. Neither methanol nor CO_2 alone can introduce nanopores into the PS-PVP thin films; however, the mixtures of methanol and CO_2 can effectively localize methanol into PVP domains and leave nanopores after removal of the mixtures. It is the key to the successful introduction of the nanopores to reduce the glass-transition temperature of PS skeleton domains by plasticizing with CO_2, which changes the properties depending on the pressure and evaporates quickly from the mixture upon depressurization. The size of the nanopores can be successfully adjusted from about 20 to 70 nm in diameter by changing the pressure of CO_2. On our experimental time scale, the morphologies in the swollen state were not equilibrium, and the resultant nanoporous structures depend on the initial morphologies before the process.

Acknowledgment. This work has been supported by a Grant-in-Aid for Scientific Research on Priority Area "Soft Matter Physics" (no. 463) from the Ministry of Education, Culture, Sports, Science and Technology.

References and Notes

(1) Burda, C.; Chen, X. B.; Narayanan, R.; El-Sayed, M. A. *Chem. Rev.* **2005**, *105*, 1025–1102.
(2) Xia, Y. N.; Rogers, J. A.; Paul, K. E.; Whitesides, G. M. *Chem. Rev.* **1999**, *99*, 1823–1848.
(3) Park, C.; Yoon, J.; Thomas, E. L. *Polymer* **2003**, *44*, 6725–6760.
(4) Fink, Y.; Winn, J. N.; Fan, S.; Michel, J.; Joannopoulos, J. D.; Thomas, E. L. *Science* **1998**, *282*, 1679–1682.
(5) Thurn-Albrech, T.; Schotter, J.; Kastle, G. A.; Emley, N.; Shibauchi, T.; Krusin-Elbaum, L.; Guarini, K.; Black, C. T.; Tuominen, M. T.; Russell, T. P. *Science* **2000**, *290*, 2126–2129.
(6) Pai, R. A.; Humayun, R.; Schulberg, M. T.; Sengupta, A.; Sun, J. N.; Watkins, J. J. *Science* **2004**, *303*, 507–510.
(7) Kim, D. H.; Kim, S. H.; Lavery, K.; Russell, T. P. *Nano. Lett.* **2004**, *4*, 1841–1844.
(8) Olson, D. A.; Chen, L.; Hillmyer, M. A. *Chem. Mater.* **2008**, *20*, 869–890.
(9) DeSimone, J. M. *Science* **2002**, *297*, 799–803.
(10) Reverchon, E.; Adami, R. *J. Supercrit. Fluid* **2006**, *37*, 1–22.
(11) Zhang, H. F.; Long, J.; Cooper, A. I. *J. Am. Chem. Soc.* **2005**, *127*, 13482–13483.
(12) Cooper, A. I. *Adv. Mater.* **2003**, *15*, 1049–1059.
(13) Cooper, A. I. *J. Mater. Chem.* **2000**, *10*, 207–234.
(14) Yokoyama, H.; Li, L.; Nemoto, T.; Sugiyama, K. *Adv. Mater.* **2004**, *16*, 1542–1546.
(15) Li, L.; Yokoyama, H.; Nemoto, T.; Sugiyama, K. *Adv. Mater.* **2004**, *16*1226–1229.
(16) Li, L.; Nemoto, T.; Sugiyama, K.; Yokoyama, H. *Macromolecules* **2006**, *39*, 4746–4755.
(17) Yokoyama, H.; Li, L.; Dutriez, C.; Iwakura, Y.; Sugiyama, K.; Masunaga, H.; Sasaki, S.; Okuda, H. *Macromolecules* **2008**, *41*, 8626–8631.
(18) Guarini, K. W.; Black, C. T.; Yeung, H. I. *Adv. Mater.* **2002**, *14*, 1290–1293.
(19) Xu, T.; Stevens, J.; Villa, J.; Goldbach, J. T.; Guarini, K. W.; Black, C. T.; Hawker, C. J.; Russell, T. P. *Adv. Funct. Mater.* **2003**, *13*, 698–702.
(20) Xu, T.; Goldbach, J. T.; Misner, M. J.; Kim, S.; Gibaud, A.; Gang, O.; Ocko, B.; Guarini, K. W.; Black, C. T.; Hawker, C. J.; Russell, T. P. *Macromolecules* **2004**, *37*, 2972–2977.
(21) Peng, J.; Kim, D. H.; Knoll, W.; Xuan, Y.; Li, B. Y.; Han, Y. C. *J. Chem. Phys.* **2006**, *125*, 064702.
(22) Tomasko, D. L.; Li, H. B.; Liu, D. H.; Han, X. M.; Wingert, M. J.; Lee, L. J.; Koelling, K. W. *Ind. Eng. Chem. Res.* **2003**, *42*, 6431–6456.
(23) Yokoyama, H.; Kramer, E. J.; Hajduk, D. A.; Bates, F. S. *Macromolecules* **1999**, *32*, 3353–3359.
(24) Ohgaki, K.; Katayama, T. *J. Chem. Eng. Data* **1976**, *21*, 53–55.
(25) Yokoyama, H.; Mates, T. E.; Kramer, E. J. *Macromolecules* **2000**, *33*, 1888–1898.
(26) Wang, W. C. V.; Kramer, E. J.; Sachse, W. H. *J. Polym. Sci., Polym. Phys. Ed.* **1982**, *20*, 1371–1384.
(27) Zhang, Y.; Gangwani, K. K.; Lemert, R. M. *J. Supercrit. Fluid* **1997**, *11*, 115–134.
(28) Washiyama, J.; Creton, C.; Kramer, E. J.; Xiao, F.; Hui, C. Y. *Macromolecules* **1993**, *26*, 6011–6020.

MA900123E